Environmental Science Processes & Impacts

PAPER

View Article Online
View Journal | View Issue

Cite this: *Environ. Sci.: Processes Impacts*, 2025, **27**, 2865

Chemical proteomics reveals human liver fatty acid binding protein as a predominant and selective target of triphenyl phosphate

Jolie Miller, [a] Jiajun Han,[a] Diwen Yang, [b] Miriam L. Diamond, [cd] Runzeng Liu *[a] and Hui Peng *[ade]

Received 28th April 2025
Accepted 10th August 2025

DOI: 10.1039/d5em00327j

rsc.li/espi

Triphenyl phosphate (TPHP) is a commonly used flame retardant and plasticizer with well-documented toxicity at environmentally relevant concentrations. We tested the hypothesis of covalent protein binding as a mechanism of TPHP toxicity by using chemical proteomics to identify adducted targets from human and rat hepatic proteomes. Results *via* in-gel fluorescent imaging showed that the TPHP-probe covalently bound many proteins with substantial interspecies variation. Using shotgun proteomics, we confirmed liver carboxylesterases as major targets in rat liver but identified liver fatty acid binding protein (L-FABP) as a novel and predominant target in human liver cells. The binding of TPHP to L-FABP was also confirmed by using recombinant L-FABP protein. We confirmed that TPHP binding to L-FABP is structurally selective, demonstrating that aryl side chains and the phosphate ester center are both essential for binding. Thus, we conclude that L-FABP is a predominant and selective target of TPHP in human hepatic proteome and that covalent protein adduction is an understudied toxicity mechanism for TPHP, presenting concerns regarding its widespread usage.

Environmental significance

Triphenyl phosphate (TPHP) is a commonly used flame retardant and plasticizer but its toxicity mechanism remains unclear. While noncovalent binding to nuclear receptors has been suggested as a potential toxic model of action, their relatively low binding affinity (generally, K_D > 10 μM) cannot fully explain the toxicity of TPHP at environmentally relevant concentrations. We herein employed chemical proteomics and discovered covalent protein adduction as a previously ignored toxicity pathway for aryl organophosphate flame retardants. Moreover, liver fatty acid binding protein was identified and validated as the predominant hepatic protein target for TPHP in both rat and human.

1. Introduction

Organophosphate esters (OPEs) are commonly used as plasticizers and flame retardants, with global use increasing significantly in recent years as they replaced brominated flame retardants.[1] However, OPEs may be a regrettable substitution due to their numerous suspected health effects,[2] including endocrine-disrupting activity,[3] developmental toxicity[4,5] and neurotoxicity.[6] OPEs can be broadly classified into three categories based on differences in structure, namely *via* R-groups: alkyl, aryl, and halogenated, each with overlapping but distinct toxicological profiles.[7] Triphenyl phosphate (TPHP) is an aryl phosphate and one of the most commonly used flame retardants in many polymers, partially due to its dual-use as a plasticizer.[8] TPHP has been widely detected in indoor dust,[9] surface water,[10] drinking water,[11] outdoor air,[12] wildlife tissues[13] and human blood,[14] making the study of its potential toxicity increasingly relevant. TPHP is most prevalent in the indoor environment, with the Canadian House Dust Study detecting it in 99.4% of samples (n = 818), with a max. of 91 000 ng g^{-1}.[15] Various adverse health effects have been associated with TPHP exposures, even at environmentally relevant concentrations,[7,16,17] but its toxicity mechanisms remain unclear.[18]

While previous molecular toxicology research on OPEs has largely focused on noncovalent binding to nuclear receptors, their relatively low binding affinity (*e.g.*, K_D ∼ 579 μM between TPHP and PPARγ)[19] cannot fully explain their toxicity at environmentally relevant concentrations. Structurally similar organophosphorus pesticides are known to cause toxicity through covalent adduction to acetylcholinesterase,[19] as well as many other serine hydrolases[20] and carboxylesterases.[21] Covalent binding to proteins is of particular concern, as irreversible

[a]*Department of Chemistry, University of Toronto, Toronto, ON, M5S 3H6, Canada. E-mail: rz.liu@sdu.edu.cn; hui.peng@utoronto.ca*

[b]*Department of Physical and Environmental Sciences, University of Toronto, Scarborough, ON, M1C 1A4, Canada*

[c]*Department of Earth Sciences, University of Toronto, Toronto, ON, M5S 3B1, Canada*

[d]*School of the Environment, University of Toronto, Toronto, ON, M5S 3H6, Canada*

[e]*Structural Genomics Consortium (SGC), University of Toronto, Toronto, ON, M5S 3H6, Canada*

protein adducts can be continuously accumulated[22] through long-term and low-dose exposure to chemical contaminants. While it was expected that this toxicity mechanism would not extend to organophosphate ester flame retardants due to the decreased capacity of their esters to act as leaving groups, a previous study determined that TPHP can bind to and inhibit carboxylesterase (CES) proteins in mice, with a potentially covalent mechanism.[23] Following studies further confirmed the inhibition of human CES proteins by a broad spectrum of OPEs.[17,24,25] While these pilot studies highlighted covalent protein binding as a potential toxicity mechanism for OPEs, it remains unknown whether other human proteins beyond CES proteins might be attacked *via* a similar covalent mechanism.

In this study, we employed a TPHP-alkyne probe and an activity-based protein profiling (ABPP) approach to systematically investigate the hepatic proteome reactivity of TPHP in human (represented by HepG2 hepatic cell line) and rat (*Rattus norvegicus*). We discovered widespread protein adduction by TPHP with significant interspecies differences, and identified liver fatty acid binding protein (L-FABP) as a novel and specific target of TPHP. Taken together, our results suggest covalent protein binding as an understudied mechanism of toxicity for OPEs, particularly aryl-OPEs, and that it may increase usage concern for certain OPEs.

2. Materials and methods

2.1 Synthesis of alkyne triphenyl phosphate probe

The synthesis of the TPHP-probe was conducted under N_2 atmosphere. Diphenyl phosphoryl chloride (3.8 mmol, CAS: 2524-64-3) was added to 10 mL of toluene in a conical flask, after which 3.8 mmol of 3-hydroxyphenylacetylene (CAS: 10401-11-3) and 1.5 mL of diisopropylethylamine were added. The reaction was stirred at room temperature for 16 hours, then quenched by addition of 35 mL of aqueous sodium bicarbonate. Organics in the reaction solution were extracted with ethyl acetate (EtAc), dehydrated with Na_2SO_4, and dried under N_2 blow-down at 40 °C. The crude product was then collected and purified, with identity and purity assessed using both ^{1}H-NMR and LC-MS/MS (details in SI and Fig. S1).

2.2 CES1 activity assay

The hydrolase activity of CES1 was determined as described previously using a *p*-nitrophenyl acetate (PNPA) as substrate.[26] The stock CES1 lysate was aliquoted to a 96-well plate and diluted to 10 μg mL^{-1} with 100 μL phosphate buffer (137 mM sodium chloride, 10 mM phosphate buffer, 2.7 mM potassium chloride, pH 7.4). The maximal final concentration was 5 μM for TPHP or TPHP-probe with a 4-fold serial dilution to obtain the lower inhibitor concentrations. Triplicates samples were conducted for each concentration of substrate. Then the reaction was initiated by the addition of 100 μM PNPA after a 2-minute preincubation at 37 °C. After 10 min, the formed *p*-nitrophenol (PNP) was measured by absorbance at 410 nm using a plate reader.

2.3 Activity-based protein profiling (ABPP) on cell lysates

We first employed in-gel fluorescence-based ABPP to directly visualize the potential proteins adducted by TPHP-probe. To achieve this, the TPHP-probe was first incubated with protein lysates, then labeled proteins were further subjected to click chemistry to be linked to a fluorescent chromophore (Fig. 2A). The fluorescent labeled proteins were further visualized by using SDS-PAGE and in-gel fluorescence imaging. As extensive washing and SDS-PAGE conditions were used in the approach, nonspecific or noncovalent binding was minimized while covalently labeled proteins were maintained for visualization.

In brief, crude protein extracts (extraction procedure in SI) from HepG2 or rat liver tissue lysate were aliquoted into PBS at 35 μg protein per replicate for negative controls (with or without click cocktail), and 3 × 35 μg protein per experimental stock tube. Then, TPHP-probe was added to experimental stock tubes for a final concentration of 100 μM, and all tubes were shaken at room temperature for 1 h. After this, a fluorophore-azide "click cocktail" was added to both experimental and negative control tubes for a final concentration of 1 mM $CuSO_4$, 1 mM TCEP, 0.1 mM THPTA, and 0.1 mM Alexa Fluor™ 488 Azide, and tubes were shaken at RT for 1 h. Reactions were then quenched with five volumes of ice-cold acetone overnight, then centrifuged (14 000 rcf, 4 °C, 10 min) to pellet proteins. Pellets were further rinsed twice with ice cold acetone before being allowed to air dry. SDS-PAGE and fluorescent imaging methods can be found in the Materials and methods section of the SI. All animal procedures were performed in accordance with the Guidelines for Care and Use of Laboratory Animals of the University of Toronto and approved by the Animal Ethics Committee of the University of Toronto.

2.4 Biotin affinity pulldown and peptide purification

To identify bound proteins, we utilized biotin-affinity based protein purification, where proteins were first reacted with the TPHP-probe, then incubated with biotin-azide on a streptavidin bead scaffold before washing and trypsin digestion. The resulting tryptic peptides were run through nanoLC-MS/MS for identification (Fig. 3A). To identify TPHP-adducted proteins with confidence, we included a negative protein lysate control treated and analyzed by the same methods without TPHP-probe incubation.

Experimental tubes and negative control tubes were prepared in triplicate, as well as one crude protein extract tube (all 150 μg protein in PBS). 100 μM TPHP-probe was added to experimental tubes, and all tubes were shaken at RT for 1 h. After this, a biotin-azide "click cocktail" was added to both experimental and negative control tubes for a final concentration of 1 mM $CuSO_4$, 1 mM TCEP, 0.1 mM THPTA, and 0.1 mM biotin azide, and tubes were shaken at RT for 1 h. Reactions were then quenched with five volumes of ice-cold acetone overnight, then centrifuged (14 000 rcf, 4 °C, 10 min) to pellet denatured proteins. Pellets were further rinsed twice with ice cold acetone to remove nonspecific binding before being allowed to air dry. At this point, the crude extract tube was reconstituted in 100 μL 50 μM ammonium bicarbonate buffer

and set aside at 4 °C. All other protein pellets were reconstituted in 50 μL 1% SDS in PBS, heated 10 minutes at 95 °C, then spun down (1000 rcf, 3 min). This heat-spin cycle was repeated until the pellet was fully redissolved, with a higher intensity for the final centrifugation (12 000 rcf, 10 min). The supernatant was then removed and added to sample tubes containing 430 μL PBS and 60 μL pre-washed streptavidin resin. Tubes were laid horizontally in a heated shaker and gently mixed for 90 min (200 rcf, 37 °C) before samples were pelleted and washed (twice with 500 μL 0.1% SDS in PBS, twice with 500 μL PBS, five minutes each with gentle shaking). The final pellet was reconstituted in 100 μL 50 μM ammonium bicarbonate, then (with crude extract tube reintroduced), an overnight on-bead trypsin digestion (200 rcf, 37 °C) was performed prior to sample analysis *via* nano-LC separation and detection on a Q-Exactive HF-X Orbitrap mass spectrometer (details in SI).

2.5 Proteomics data analysis

Raw proteomics data files were analyzed using MaxQuant version 1.6.0.16, and extracted MS/MS spectra were matched using the Andromeda search engine against tryptic peptides (min. peptide length of 7 and max. of two missed cleavages) derived from the human reference proteome (Uniprot, accessed 2018/09) or the brown rat reference proteome (Uniprot, accessed 2017/03) and a list of common contaminants. Unless noted otherwise, parameters were kept at default settings with a false discovery rate of 1% at the peptide and protein levels. "Re-quantify" and "match between runs" were selected to maximize true protein discovery. Downstream data analysis was conducted in Microsoft Excel version 2312. In both rat and human experiments, any proteins or peptides identified mainly as potential contaminants, reverse, or only identified by site were discarded prior to further analysis.

For biotin-affinity experiments, TPHP-probe adducted proteins were identified based on relative intensity of peptides present in experimental samples *versus* control samples. The 'proteinGroups.txt' output from MaxQuant was imported into Excel and after initial filtering, samples were grouped based on exposure and technical replicates. For each protein group, the relative intensity was determined based on total sample intensity for that replicate (with '0' values replaced with '10 000'). Fold-change and *p*-value were then calculated between the experimental and negative control replicates, with *p*-value calculated using a paired, two-tailed Student's *t*-test. We considered protein groups with an intensity fold-change ≥ 5 times that of the negative control and a *p*-value ≤ 0.05 to be significantly adducted by the TPHP-probe. At this point, we excluded protein identifications based only on detection of a single peptide.

The proteomics datasets generated and analyzed during this study have been deposited to the ProteomeXchange Consortium under the identifier PXD057684.

2.6 ABPP competition assay with pure hL-FABP

To confirm binding of native TPHP to purified recombinant hL-FABP (expression and purification procedure found in SI), an in-gel competition assay was prepared with varied concentrations of TPHP against a constant concentration of hL-FABP and TPHP-probe. Tubes were prepared in duplicate with 7.5 μM hL-FABP, plus 30, 60, or 120 μM TPHP, and 30 μM TPHP-probe. Additional duplicates with only 7.5 μM hL-FABP and 30 μM TPHP or TPHP-probe were included, as well as a negative control containing only 7.5 μM hL-FABP. To start the reaction, either TPHP or DMSO was added to each hL-FABP tube, which were then shaken for 1 hour at RT. This process was repeated with the additions of the TPHP-probe (added to specified tubes), then Azide-Fluor 488 click cocktail (added to all tubes). Reactions were then quenched with five volumes of ice-cold acetone overnight at −20 °C, then centrifuged (14 000 rcf, 4 °C, 10 min) to pellet proteins. Pellets were further rinsed twice with ice cold acetone before being allowed to air dry, then proteins were visualized *via* SDS-PAGE and fluorescence imaging.

2.7 ANS assay

The relative binding affinities of OPEs to human liver FABP and human epithelial FABP were determined using a fluorescent displacement assay with 1,8-ANS. A serial dilution of OPEs (11 concentrations, 0.15–153.6 μM) were prepared in triplicate in ANS buffer (50 mM Tris, 150 mM NaCl, 1 mM DTT, pH 8) with 40 μM ANS (negative control) or in ANS buffer with 40 μM ANS and 1 μM hL-FABP or hE-FABP in a Nunc white chimney 96-well plate. DMSO was added in triplicate as a 0 μM OPE vehicle control. The plate was then shaken at 125 rcf for 1 h at room temp prior to fluorescent imaging (details in SI). Data analysis was performed in GraphPad Prism 10.1.2, using a nonlinear [inhibitor] *vs.* response model with four variables. All 50% 1,8-ANS displacement values were calculated *via* eqn (S1) with values from Table S1.

3. Results and discussion

3.1 Synthesis and validation of an alkyne TPHP-probe

To test the hypothesis of covalent protein adduction as a mechanism of OPE toxicity (Fig. 1A), we synthesized a TPHP-probe with an alkyne handle (Fig. 1B) to profile its proteome binding by using an activity-based protein profiling (ABPP) approach. Alkyne groups are the most commonly used chemical handle for ABPP as their small size and biorthogonal nature minimizes off-target binding and maintains bioactivity,[27] as well as their ease of use with click-chemistry. To confirm that the bioactivity of TPHP-probe was conserved relative to native TPHP, we used a CES1 enzymatic assay for validation, as CES1 is a well-established target for TPHP.[23,26,28] The CES1 inhibition activity of TPHP-probe ($IC_{50} = 1.14$ nM) is comparable to that of native TPHP ($IC_{50} = 4.67$ nM) (Fig. 1C). This demonstrated that the addition of a small alkyne group to TPHP does not impact its binding to CES1, supporting the use of our TPHP-probe as a chemically analogous TPHP substitute for ABPP.

3.2 The TPHP-probe adducted the hepatic proteome in both human and rat

Due to the well-documented role of the liver in mediating OPE toxicity,[29] we chose to investigate interspecies TPHP binding

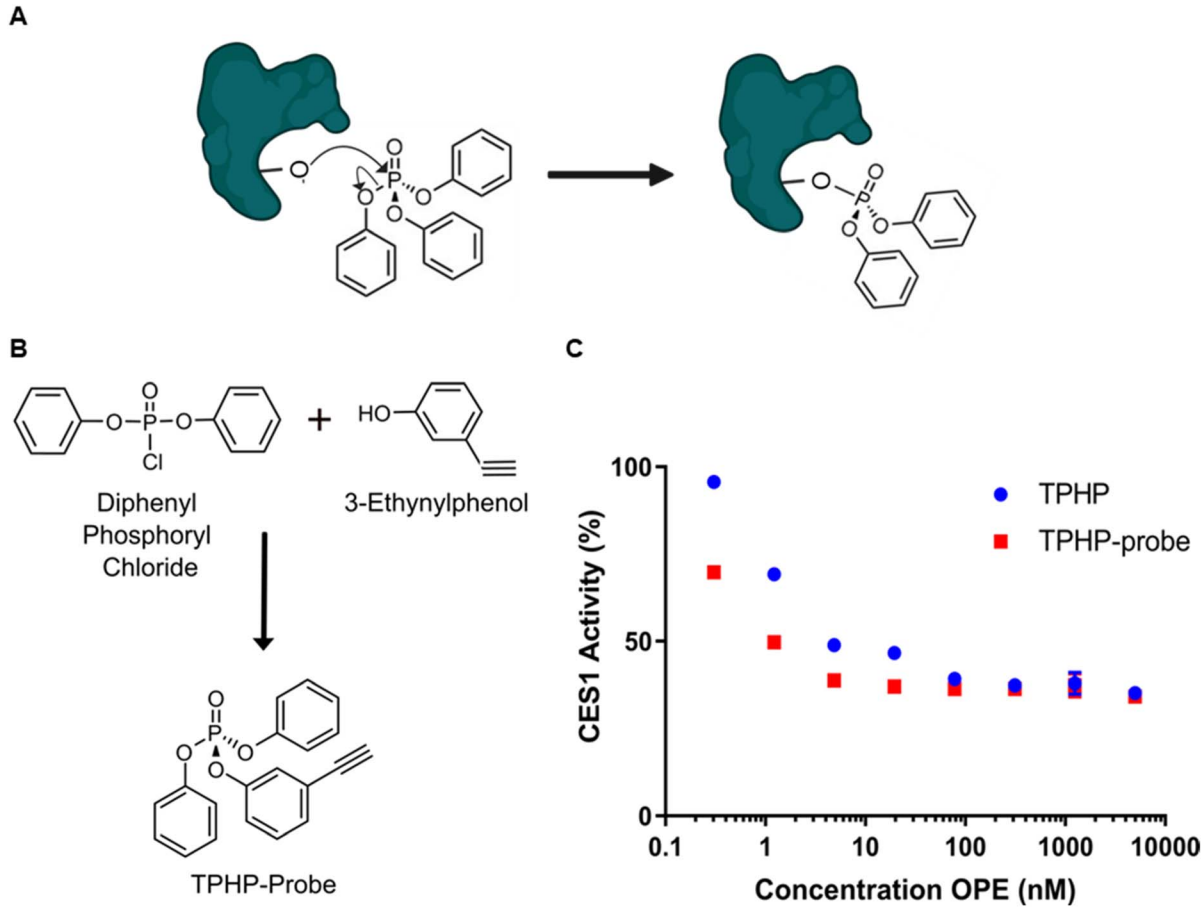

Fig. 1 Synthesis and benchmarking an alkyne TPHP-probe. (A) Illustration of hypothesis that TPHP forms covalent adduct with nucleophilic amino acid residues (*e.g.*, serine). (B) Synthesis of the TPHP-probe with an alkyne handle. (C) Native TPHP and alkyne TPHP-probe exhibit similar CES inhibition activities ($N = 3$).

differences within the hepatic proteome. Compared to traditional *in vivo* toxicity testing relying on animal models, chemical proteomics approaches provide a convenient way to characterize bioactivity mechanisms by using cell lines or tissue samples.[30] To take advantage of this aspect of ABPP, we investigated the protein-binding profiles of the TPHP-probe in both humans and rats for comparison, by directly visualizing their liver tissue (rat) or cell line crude protein lysates (human) in complex with our TPHP-probe and fluorophore (see workflow in Fig. 2A).

During the initial test with rat liver tissue lysate, we found that the TPHP-probe bound to many proteins in comparison to the negative control (containing only azide-fluorophore in the absence of TPHP-probe; Fig. 2B). To test whether TPHP protein labeling was selective, we stained the gel with Coomassie blue dye to visualize protein abundance post fluorescence imaging. Notably, we did not observe a direct correlation between fluorescence intensity and Coomassie staining, indicating that protein binding was specific and varied in affinity between proteins, instead of nonspecific binding (which would vary proportionally with protein abundance). For instance, the ~60 kDa rat protein band had a much higher fluorescent intensity than all others in the gel after TPHP-probe labeling, but it had a lower relative intensity in the Coomassie stained gel. Thus, while this band was not present at extremely high abundance compared to other proteins, it had a very high TPHP-binding affinity. We hypothesize that the band at ~60 kDa corresponds to the well-documented TPHP targets CES1 and CES2 proteins, both with molecular weights of ~63 kDa. Collectively, these results demonstrated that the ABPP approach can be directly used to visualize the proteome binding profile of TPHP in liver tissue lysates.

Next, we tested ABPP in human HepG2 cells. As in the rat hepatic proteome, the TPHP-probe adducted many human hepatic proteins. Notably, large interspecies variations were observed as shown by differences in fluorescence intensity. For instance, the suspected CES protein band (~60 kDa) was detected in human protein lysate with a lower relative fluorescence intensity in comparison to the rat band, indicating TPHP-binding at a lower level than in rat liver lysate. Taken together, the in-gel fluorescence results demonstrated that TPHP covalently reacts with a broad spectrum of hepatic proteins, with a large interspecies variation between human and rat hepatic proteomes.

3.3 Chemical proteomics identification of hL-FABP as a predominant target of TPHP in human hepatic proteome

After confirmation of TPHP-protein adduction *via* the in-gel fluorescence results, we moved forward by using shotgun

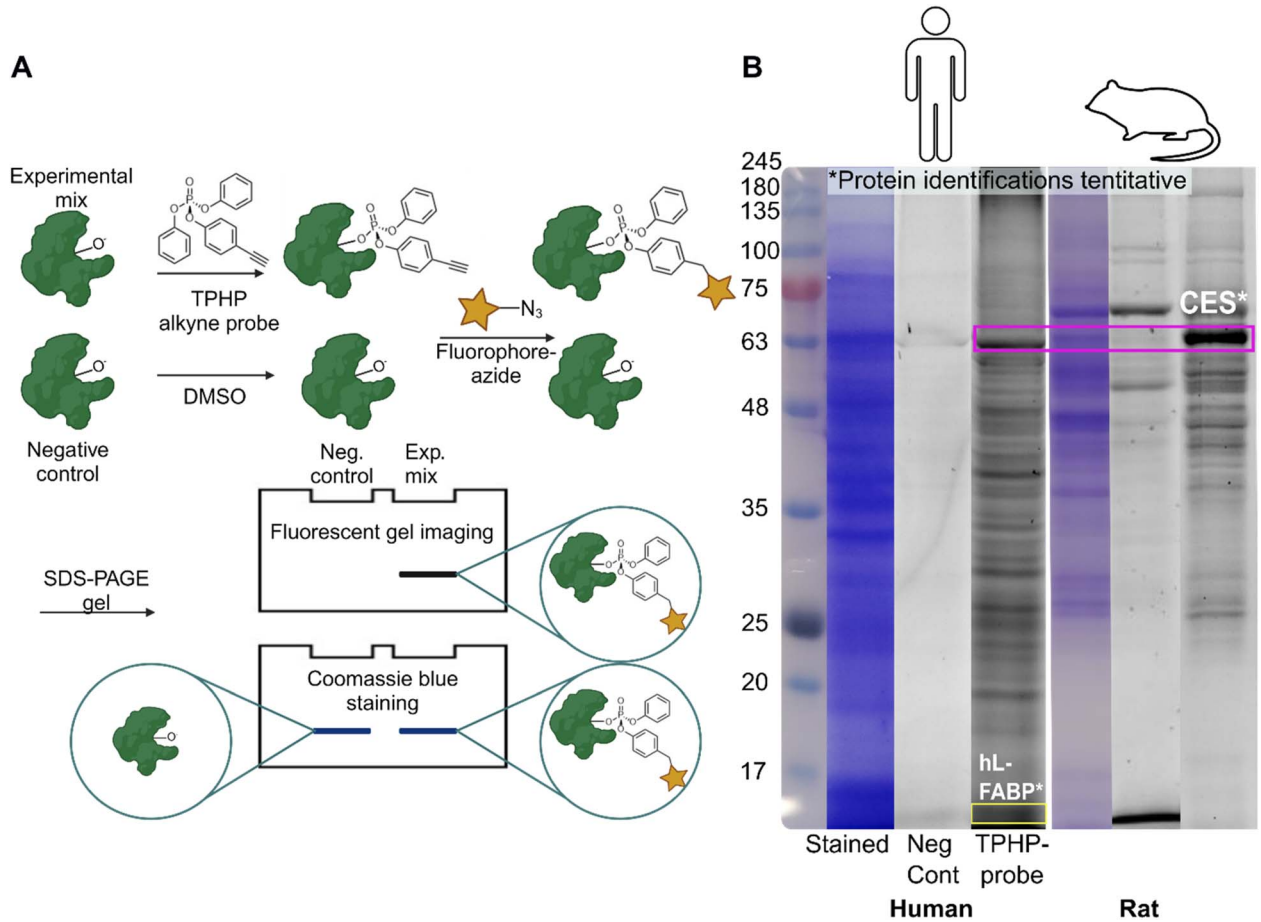

Fig. 2 TPHP-probe reacts with hepatic proteome in both human and rat. (A) ABPP allows visualization of proteins labeled by the TPHP-alkyne probe. (B) TPHP-probe reacts with hepatic proteomes across species. Results are shown from TPHP-probe exposure to liver proteomes from human and rat. Suspected protein bands from CEH B1 proteins (~60 kDa) are highlighted. For each species, rows were shown in the order of 'Stained', 'Neg Cont', and 'TPHP-probe'. Stained = Coomassie blue stained TPHP-probe exposed lysate, Neg Cont = fluorescent image of lysate without TPHP-probe, TPHP-probe = fluorescent image of lysate exposed to TPHP-probe.

proteomics to precisely identify the protein targets covalently labeled by the TPHP-probe (see workflow in Fig. 3A). A relatively high concentration of probe (100 μM) was chosen as an experimental concentration to improve the sensitivity and signal-to-noise ratio of our method, as we aim to determine protein targets on the proteome-wide level without discrimination based on affinity.

We first applied the ABPP approach to rat liver tissue lysates to validate this chemical proteomics method by identifying the specific CES proteins that had appeared so strongly in our in-gel fluorescence results. After filtering and data analysis (see Methods section), we identified 234 protein groups collectively in the rat biotin-affinity pulldown samples, 35 of which were considered significantly adducted by the TPHP-probe (Fig. 3B). As suspected, multiple rat CES protein groups were identified as highly adducted by our TPHP-probe, including Ces2a/Ces2j/Ces2g, Ces1f, Ces2e, and Ces1e/Ces1c (shown in green in Fig. 3B, with MS/MS spectra in Fig. S3 and S4), confirming our hypothesis that these CES proteins are predominant targets in rat hepatic proteome.

After benchmarking our ABPP chemical proteomics approach using the rat hepatic proteome, we investigated TPHP adduction within the human hepatic proteome (represented here by HepG2 cell lysate). We completed three independent trials of experiments, each in triplicate, before compiling results. In these three trials, 216 protein groups were pulled down by the TPHP-probe, with 8 significant in 1/3 trials, 1 significant in 2/3 trials, and 1 significant in all three trials (Fig. 3C). In contrast to the results from rat, liver fatty acid binding protein (hL-FABP/FABP1) was consistently detected as the top target (Fig. 3C, FABP1 bolded in black) across all 3 batches of ABPP proteomics results. The proteomics results correspond to in-gel fluorescence results where a strong protein band was observed at ~14 kDa in HepG2 (Fig. 2B), which is the expected molecular size of hL-FABP. L-FABP was also identified as a target for TPHP from rat protein affinity pulldown trials (Fig. 3B with MS/MS spectra in Fig. S5), albeit at lower signals than CES proteins. L-FABP is a highly abundant hepatic protein involved in transport and binding of fatty acids,[31] which has also been reported as critical for the hepatic accumulation of per- and polyfluoroalkyl substances (PFAS).[32] The identification

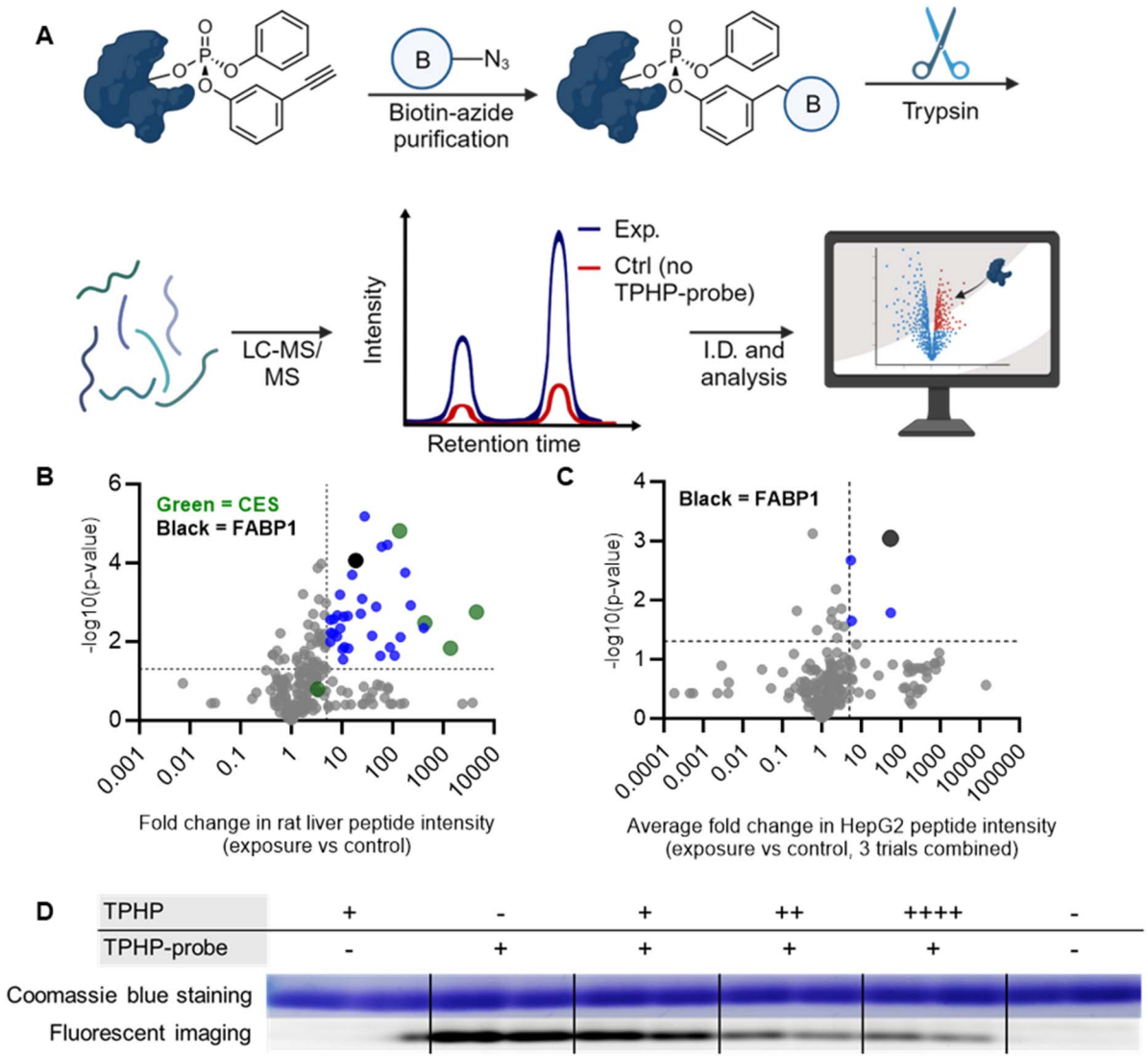

Fig. 3 Chemical proteomics identified L-FABP as a main TPHP target in human liver cells. (A) TPHP-probe adducted proteins were isolated by binding to streptavidin azide beads, prior to protein identification *via* LC-MS/MS and fold-change analysis against control. (B) In rat liver lysate, CES proteins were generally highly adducted by the TPHP-probe, as was L-FABP. (C) In HepG2 cell protein lysate, L-FABP was the only protein significantly adducted in all trials. (D) Confirmation of TPHP binding to purified recombinant hL-FABP, with a decrease in fluorescence representing displacement of TPHP-probe ($N = 2$).

of L-FABP as a novel target for TPHP was unexpected, as the tetrahedral aryl structure of TPHP differs from previously known ligands (*e.g.*, fatty acids and PFAS).[33]

To confirm TPHP binding to hL-FABP, we utilized a simple in-gel ABPP competition assay with purified recombinant hL-FABP protein. We incubated the protein with our TPHP-probe alongside various concentrations of native TPHP, then visualized relative hL-FABP adduction *via* in-gel fluorescence. As shown in Fig. 3D, purified hL-FABP was labeled by the TPHP-probe in the absence of native TPHP, confirming pulldown results. The fluorescence of the hL-FABP band decreased as concentration of native TPHP increased, confirming that both native TPHP and TPHP-probe can selectively bind to the same site of hL-FABP. This also provides evidence for a multi-step reaction in which native TPHP may be able to displace the TPHP-tag in a fast, noncovalent binding phase, prior to slow covalent bond formation. Despite extensive efforts, we were not able to identify the covalent adduction site of TPHP to L-FABP, potentially due to the labile P–O bond (see more information in Text S2). To our knowledge, this is the first time FABP1 has been identified as a direct protein target for an organophosphate ester.

3.4 hL-FABP selectively binds to aryl-OPEs

After confirming hL-FABP binding to native TPHP, we sought to determine its binding activity at lower concentrations, as well as to investigate whether other OPE compounds could also bind to hL-FABP. Our group previously used a displacement assay with the fluorescent probe 1,8-ANS to determine the binding affinities of PFAS to hL-FABP[32] (workflow is shown in Fig. S6). We

modified this fluorescence displacement assay to consider the potential for covalent binding among OPEs, with the main change being a longer incubation time with the protein.

We first tested nine commonly used OPEs from three main structural categories (*i.e.*, aryl, alkyl, and halogenated), to investigate the potential impacts of side chains on protein binding (Fig. 4 and Table S1). As expected, TPHP binds to hL-FABP relatively strongly, displacing 50% of ANS from the binding pocket at 2.73 μM. This further confirmed our ABPP chemical proteomics and in-gel fluorescence results that TPHP binds to hL-FABP. The other tri-aryl OPE, ToTP also bound with hL-FABP, with a very similar 50% displacement value at 2.69 μM. The TPHP-probe was also tested, with a very similar curve to native TPHP, but slightly lowered affinity (50% displacement at 8.55 μM, see Fig. S8). The di-aryl OPE, EHDPP, showed significant binding potential, but with a lower binding potency, only reaching around 50% relative fluorescence as compared to the tri-aryl OPEs, which displaced most of the fluorescent molecule. This difference in affinity between tri- and di-aryl OPEs suggests that even one alkyl substitution may significantly decrease binding affinity to hL-FABP. The hypothesis that alkyl substitution decreases hL-FABP binding affinity was further supported when testing tri-alkyl OPEs. All six tri-alkyl or chloroalkyl OPEs showed insignificant or weak binding to hL-FABP.

Taken together, evidence from the displacement assay suggests that R-group substitution strongly influences OPE

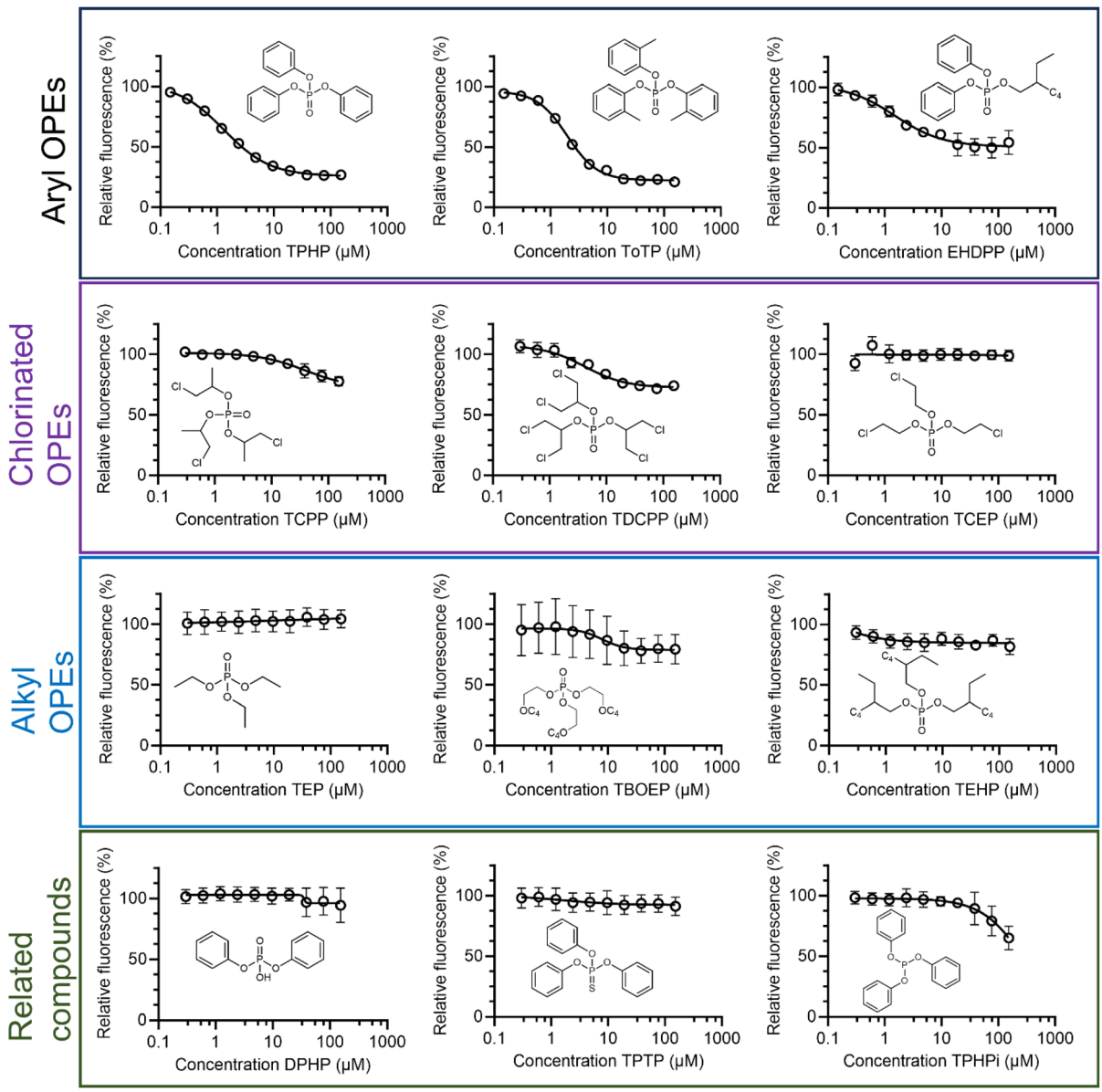

Fig. 4 Human L-FABP selectively binds to aryl-OPEs. Aryl OPEs, left to right: TPHP, ToTP, EHDPP. Chlorinated OPEs, left to right: TCPP, TDCPP, TCEP. Alkyl OPEs, left to right: TEP, TBOEP, TEHP. Related compounds, left to right: DPHP, TPTP, TPHPi. Fluorescence displacement assays of ANS from the hL-FABP binding pocket show that aryl-OPEs consistently bind inside of hL-FABP, while other OPEs and related compounds show limited to no binding affinity.

binding to hL-FABP, with aryl-groups increasing binding, and alkyl and chloroalkyl groups decreasing binding potential. This result aligns with the hypothesis of covalent adduction as a mechanism for aryl OPE-protein binding, as aryl esters will be more likely to function as leaving groups than chloroalkyl or alkyl esters, which are not resonance stabilized and therefore have a lower leaving group capacity. Additionally, these binding trends align with the general increased *in vitro* toxicity of aryl-OPEs over other OPE structural groups.[34–38] These results support covalent protein binding as a likely mechanism for the toxicity of aryl-OPEs.

After confirming the importance of OPE R-groups, we moved forward to testing the potential impact of modifications to the phosphate ester center (Fig. 4 and Table S1). We selected three structurally related compounds including diphenyl phosphate (DPHP), *O*,*O*,*O*-triphenyl phosphorothioate (TPTP) and triphenyl phosphite (TPHPi). These three compound classes are common contaminants and were selected because they are structurally similar and may transform into or from TPHP.[52,53] No binding was detected for the diester diphenyl phosphate (DPHP). This might be because the deprotonated OH group on the diester decreases the electrophilicity of the phosphorous center, making covalent adduction less likely and decreasing the leaving group ability of the remaining aryl rings. DPHP is a metabolite of TPHP, and previous studies have widely reported its presence in humans[39] and the environment.[7] Studies have also reported the toxicity of DPHP in fish[40] and mice,[41] but its toxicity is significantly lower compared to TPHP.[42] Our results supported the conclusion that the low proteome reactivity of DPHP might partially explain its generally low toxicity, especially relating to hepatotoxicity.[43]

Similar to DPHP, a low binding affinity was observed for TPTP, a thiophosphate formed from TPHPi *via* abiotic reactions.[44] This lack of binding demonstrated that the thiophosphate ester is not electrophilic enough to react with L-FABP. It is of note that many organophosphate insecticides with known covalent interactions to proteins are thiophosphates, but they must undergo a bioactivation to an oxon group before they exhibit this reactivity,[45] supporting covalent reactivity as specific to phosphate esters.

Finally, TPHPi shows little to no affinity to hL-FABP at lower concentrations but begins to show some binding at high concentrations. This compound would not be susceptible to covalent attack due to the trivalent state of phosphorus. The weak binding of TPHPi to hL-FABP could be due to a TPHP impurity which is formed *via* oxidation from TPHPi. Trivalent phosphorus is unstable when exposed to air and tends to oxidize to pentavalent phosphorus over time, resulting in decreasing concentrations of TPHPi and increasing concentrations of TPHP.[46]

Together with the structure–activity relationship, we concluded that both tri-aryl side chains and phosphate ester center of TPHP are essential for its specific binding to hL-FABP. The tri-aryl side chains are crucial to act as effective leaving groups and to form noncovalent hydrophobic and van der Waals interactions within the binding pocket, while the electron-poor phosphate center is vulnerable to covalent attack by nucleophilic amino acid residues (*e.g.*, serine). Interestingly, a similar binding was not observed for epithelial FABP, which is another protein from the same family (see Text S3, Fig. S7 and S8). Taken together, these results suggest that OPE binding is both chemical structure and protein specific.

4. Implications

In this paper, we have utilized a nontargeted method of chemical proteomics analysis to investigate and show interspecies binding differences in TPHP protein adduction, identified a significant novel TPHP protein target in the form of L-FABP, and proven a clear structural dependence for OPE binding to L-FABP. *In vivo* testing will be necessary to confirm the role of hL-FABP adduction in TPHP toxicity, but aryl-OPEs in particular are known to have obesogenic effects.[47,48] Because L-FABP is an important protein on the fatty-acid metabolism pathway,[31,49] it may be that TPHP binding to this protein leads to increased fat buildup. However, it is also possible that hL-FABP may function as a detoxification pathway *via* sequestration, as hL-FABP is highly abundant and can act as a cytotoxicity protectant.[31] *In vivo* protein knockdown studies could be used to develop a wholistic understanding of the impact of TPHP L-FABP binding.

In our current study, we have minimized non-specific and non-covalent interactions to highlight the potential for covalent protein binding as a mechanism of OPE toxicity. This mechanism of OPE toxicity is understudied but may explain multiple aspects of OPE toxicity. A structural approach to OPE toxicity investigation with a focus on covalent reactivity would help us prioritize and eliminate highly toxic OPEs, while avoiding future regrettable substitutions. Given the results of this study and high production volume and widespread wildlife and human exposure to TPHP and other aryl-OPEs,[50–52] there is an urgent need to further assess covalent binding as a potential OPE toxicity mechanism.

Conflicts of interest

There are no conflicts to declare.

Data availability

The data supporting this article have been included as part of the SI. The SI provides text, tables, and figures addressing: (1) supplementary materials and methods; (2) attempts to identify TPHP binding site within FABP1; (3) discussion of nonreactivity of aryl-OPEs with epithelial FABP; (4) characterization of TPHP-alkyne probe *via* LC-MS/MS and NMR spectra; (5) representative MS/MS *Rattus norvegicus* CES1 tryptic peptide spectra, with b and y ions labeled; (6) representative MS/MS *Rattus norvegicus* CES2 tryptic peptide spectra, with b and y ions labeled; (7) representative MS/MS *Homo sapiens* and *Rattus norvegicus* L-FABP peptide spectra, with b and y ions labeled; (8) structural confirmation of purified recombinant hL-FABP *via* top-down LC-MS; (9) 1,8-ANS assay workflow and validation of 1,8-ANS assay using PFOS; (10) nonlinear [inhibitor] *vs.* response model

with four variables, and table containing data for each ANS assay curve; (11) epithelial FABP ANS assay curves for aryl-OPEs; (12) TPHP-probe ANS assay curves for L-FABP and E-FABP. See DOI: https://doi.org/10.1039/d5em00327j.

Acknowledgements

This research was supported by the Michael J. Fox Foundation (MJFF), National Sciences and Engineering Research Council (NSERC) Discovery Grants, and Canadian Institutes of Health Research (CIHR). The authors acknowledge the support of instrumentation grants from the Canada Foundation for Innovation, the Ontario Research Fund, and the NSERC Research Tools and Instrument Grant. The authors thank Dr Carlie A. LaLone from the U.S. Environmental Protection Agency and Prof. Jon A. Doering from the Department of Environmental Sciences at Louisiana State University for providing tissue samples. Fig. 1A, 2A, and 3A were created in BioRender.

References

1 T. G. Bekele, H. Zhao, J. Yang, R. G. Chegen, J. Chen, S. Mekonen and A. Qadeer, *Environ. Sci. Pollut. Res.*, 2021, **28**, 49507–49528.
2 A. Blum, M. Behl, L. Birnbaum, M. L. Diamond, A. Phillips, V. Singla, N. S. Sipes, H. M. Stapleton and M. Venier, *Environ. Sci. Technol. Lett.*, 2019, **6**, 638–649.
3 L. Bajard, C. K. Negi, V. Mustieles, L. Melymuk, S. Jomini, J. Barthelemy-Berneron, M. F. Fernandez and L. Blaha, *Environ. Int.*, 2021, **153**, 106550.
4 C. C. Carignan, L. Mínguez-Alarcón, P. L. Williams, J. D. Meeker, H. M. Stapleton, C. M. Butt, T. L. Toth, J. B. Ford and R. Hauser, *Environ. Int.*, 2018, **111**, 232–238.
5 R. Castorina, A. Bradman, H. M. Stapleton, C. Butt, D. Avery, K. G. Harley, R. B. Gunier, N. Holland and B. Eskenazi, *Chemosphere*, 2017, **189**, 574–580.
6 H. B. Patisaul, M. Behl, L. S. Birnbaum, A. Blum, M. L. Diamond, F. S. Rojello, H. T. Hogberg, C. F. Kwiatkowski, J. D. Page, A. Soehl and H. M. Stapleton, *Environ. Health Perspect.*, 2021, **129**, 105001.
7 C. Yao, H. Yang and Y. Li, *Sci. Total Environ.*, 2021, **795**, 148837.
8 I. van der Veen and J. de Boer, *Chemosphere*, 2012, **88**, 1119–1153.
9 S. C. Hammel, K. Hoffman, A. L. Phillips, J. L. Levasseur, A. M. Lorenzo, T. F. Webster and H. M. Stapleton, *Environ. Sci. Technol.*, 2020, **54**, 4484–4494.
10 I. Pantelaki and D. Voutsa, *Sci. Total Environ.*, 2021, **800**, 149544.
11 J. Huang, J. Li, W. Meng and G. Su, *Sci. Total Environ.*, 2024, **913**, 169663.
12 R. Sühring, M. L. Diamond, M. Scheringer, F. Wong, M. Pućko, G. Stern, A. Burt, H. Hung, P. Fellin, H. Li and L. M. Jantunen, *Environ. Sci. Technol.*, 2016, **50**, 7409–7415.
13 J. Li, Y. Zhang, R. Bi, L. Ye and G. Su, *Environ. Sci. Technol.*, 2022, **56**, 302–312.
14 M. Hou, B. Zhang, S. Fu, Y. Cai and Y. Shi, *Environ. Sci. Technol.*, 2022, **56**, 8221–8230.
15 Environment and Climate Change Canada, *Draft screening assessment flame retardants group*, https://www.canada.ca/en/environment-climate-change/services/evaluating-existing-substances/draft-screening-assessment-flame-retardants-group.html, accessed 21 July 2025.
16 Y. Li, C. Wang, F. Zhao, S. Zhang, R. Chen and J. Hu, *Environ. Sci. Technol. Lett.*, 2018, **5**, 649–654.
17 B. Schmandt, M. Diduff, G. Smart and L. M. Williams, *Toxics*, 2024, **12**, 368.
18 L. Ye, J. Li, S. Gong, S. M. Herczegh, Q. Zhang, R. J. Letcher and G. Su, *J. Hazard. Mater.*, 2023, **459**, 132095.
19 L. Sun, X. Liu, J. Du, H. Yang, Y. Lin, D. Yu, C. Li and Y. Zheng, *Environ. Sci. Technol.*, 2024, **58**, 18631–18641.
20 T. Elersek and M. Filipic, in *Pesticides – The Impacts of Pesticides Exposure*, ed. M. Stoytcheva, InTech, 2011.
21 N. Lenfant, Y. Bourne, P. Marchot and A. Chatonnet, *Chem.-Biol. Interact.*, 2016, **259**, 343–351.
22 K. S. Abass, *Spectrosc. Lett.*, 2015, **48**, 265–273.
23 J. Singh, R. C. Petter, T. A. Baillie and A. Whitty, *Nat. Rev. Drug Discovery*, 2011, **10**, 307–317.
24 P. J. Morris, D. Medina-Cleghorn, A. Heslin, S. M. King, J. Orr, M. M. Mulvihill, R. M. Krauss and D. K. Nomura, *ACS Chem. Biol.*, 2014, **9**, 1097–1103.
25 G.-L. Wei, D.-Q. Li, M.-N. Zhuo, Y.-S. Liao, Z.-Y. Xie, T.-L. Guo, J.-J. Li, S.-Y. Zhang and Z.-Q. Liang, *Environ. Pollut.*, 2015, **196**, 29–46.
26 J. Du, H. Li, S. Xu, Q. Zhou, M. Jin and J. Tang, *Environ. Sci. Pollut. Res.*, 2019, **26**, 22126–22136.
27 W. Chen, Y. Gong, M. McKie, H. Almuhtaram, J. Sun, H. Barrett, D. Yang, M. Wu, R. C. Andrews and H. Peng, *Environ. Sci. Technol.*, 2022, **56**, 14627–14639.
28 S. L. Scinto, D. A. Bilodeau, R. Hincapie, W. Lee, S. S. Nguyen, M. Xu, C. W. am Ende, M. G. Finn, K. Lang, Q. Lin, J. P. Pezacki, J. A. Prescher, M. S. Robillard and J. M. Fox, *Nat. Rev. Methods Primers*, 2021, **1**, 1–23.
29 A. L. Phillips and H. M. Stapleton, *Toxicol. Sci.*, 2019, **171**, 396–405.
30 Z. Du, Y. Zhang, G. Wang, J. Peng, Z. Wang and S. Gao, *Sci. Rep.*, 2016, **6**, 21827.
31 J. Han, J. Fu, J. Sun, D. R. Hall, D. Yang, D. Blatz, K. Houck, C. Ng, J. Doering, C. LaLone and H. Peng, *Environ. Sci. Technol.*, 2021, **55**, 9012–9023.
32 G. Wang, H. L. Bonkovsky, A. de Lemos and F. J. Burczynski, *J. Lipid Res.*, 2015, **56**, 2238–2247.
33 D. Yang, J. Han, D. R. Hall, J. Sun, J. Fu, S. Kutarna, K. A. Houck, C. A. LaLone, J. A. Doering, C. A. Ng and H. Peng, *Environ. Sci. Technol.*, 2020, **54**, 5676–5686.
34 J. Thompson, A. Reese-Wagoner and L. Banaszak, *Biochim. Biophys. Acta, Mol. Cell Biol. Lipids*, 1999, **1441**, 117–130.
35 Y. Le, H. Shen, Z. Yang, D. Lu and C. Wang, *Environ. Pollut.*, 2021, **274**, 116541.
36 Z. Hao, Z. Zhang, D. Lu, B. Ding, L. Shu, Q. Zhang and C. Wang, *Chem. Res. Toxicol.*, 2019, **32**, 1250–1258.
37 X. Ji, N. Li, M. Ma, K. Rao and Z. Wang, *Sci. Total Environ.*, 2020, **727**, 138484.

38 A. K. Rosenmai, S. B. Winge, M. Möller, J. Lundqvist, E. B. Wedebye, N. G. Nikolov, H. K. Lilith Johansson and A. M. Vinggaard, *Chemosphere*, 2021, **263**, 127703.
39 J. Li, H. Cao, Y. Mu, G. Qu, A. Zhang, J. Fu and G. Jiang, *Environ. Sci. Technol.*, 2020, **54**, 14525–14534.
40 M. Ospina, N. K. Jayatilaka, L.-Y. Wong, P. Restrepo and A. M. Calafat, *Environ. Int.*, 2018, **110**, 32–41.
41 Q. Chen, X. Lian, J. An, N. Geng, H. Zhang, J. K. Challis, Y. Luo, Y. Liu, G. Su, Y. Xie, Y. Li, Z. Liu, Y. Shen, J. P. Giesy and Y. Gong, *Environ. Sci. Technol.*, 2021, **55**, 13122–13131.
42 S. Selmi-Ruby, J. Marín-Sáez, A. Fildier, A. Buleté, M. Abdallah, J. Garcia, J. Deverchère, L. Spinner, B. Giroud, S. Ibanez, T. Granjon, C. Bardel, A. Puisieux, B. Fervers, E. Vulliet, L. Payen and A. M. Vigneron, *Environ. Health Perspect.*, 2020, **128**, 127006.
43 P. D. Noyes, D. E. Haggard, G. D. Gonnerman and R. L. Tanguay, *Toxicol. Sci.*, 2015, **145**, 177–195.
44 J. Yue, X. Sun, X. Duan, C. Sun, H. Chen, H. Sun and L. Zhang, *Environ. Int.*, 2023, **172**, 107749.
45 W. Chen, H. Almuhtaram, R. Andrews and H. Peng, *ChemRxiv*, 2023, preprint, DOI: **10.26434/chemrxiv-2023-20bx2**.
46 C. M. Thompson, J. M. Prins and K. M. George, *Environ. Health Perspect.*, 2010, **118**, 11–19.
47 R. Liu and S. A. Mabury, *Environ. Sci. Technol.*, 2019, **53**, 1805–1811.
48 G. Cano-Sancho, A. Smith and M. A. La Merrill, *Toxicol. In Vitro*, 2017, **40**, 280–288.
49 A. J. Green, J. L. Graham, E. A. Gonzalez, M. R. La Frano, S.-S. E. Petropoulou, J.-S. Park, J. W. Newman, K. L. Stanhope, P. J. Havel and M. A. La Merrill, *Reprod. Toxicol.*, 2017, **68**, 119–129.
50 B. P. Atshaves, G. G. Martin, H. A. Hostetler, A. L. McIntosh, A. B. Kier and F. Schroeder, *J. Nutr. Biochem.*, 2010, **21**, 1015–1032.
51 European Chemicals Agency, *Substance Information – ECHA*, **https://echa.europa.eu/substance-information/-/substanceinfo/100.003.739**, accessed 3 July 2024.
52 Environment and Climate Change Canada, *Risk management scope for TPHP, BPDP, BDMEPPP, IDDP, IPPP and TEP*, **https://www.canada.ca/en/environment-climate-change/services/evaluating-existing-substances/risk-management-scope-tphp-bpdp-bdmeppp-iddp-ippp-tep.html**, accessed 19 December 2023.
53 R. Sühring, M. L. Diamond, S. Bernstein, J. K. Adams, J. K. Schuster, K. Fernie, K. Elliott, G. Stern and L. M. Jantunen, *Environ. Sci. Technol.*, 2021, **55**, 304–312.

